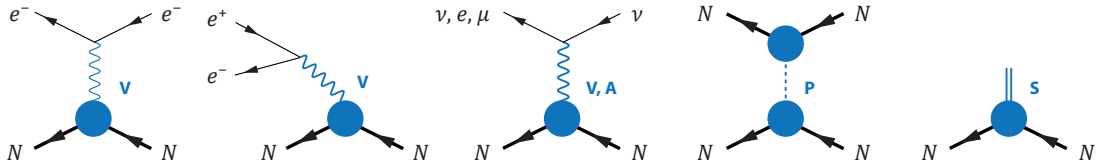

FIG. 4.15: Experimental processes involving the nucleon and different types of currents.

4.5 Hadron matrix elements

4.5.1 Scattering amplitudes

Since quarks and gluons are confined in hadrons, we cannot probe them directly in experiments. Instead, we can learn about their dynamics by probing hadrons with external currents, e.g. when scattering leptons off hadrons, or by scattering hadrons on other hadrons. Among the basic observables extracted from such reactions are the **form factors** of hadrons, which encode their momentum-dependent interactions with photons, W and Z bosons. Some of the relevant processes involving the nucleon are shown in Fig. 4.15:

- $\boldsymbol{e^-N}$ **scattering** has been essential for learning about the substructure of the proton. Due to the smallness of the electromagnetic coupling constant $\alpha_{\rm QED} \approx 1/137$, the process is dominated by one-photon exchange. The pioneering experiments by Robert Hofstadter revealed that the proton and neutron are not pointlike; instead, their **electromagnetic form factors** provide information on their substructure in terms of electric charge and magnetization distributions (Nobel prize 1961). Even today, the nucleon's electromagnetic form factors are not fully understood, as evidenced by the proton radius puzzle and other open questions. The emission/absorption of virtual photons can also turn a nucleon into a resonance, and electromagnetic **transition form factors** provide insight on the internal structure of nucleon resonances (N^*). Moreover, crossing symmetry implies that the same form factors describing the interaction with a virtual photon also enter in crossed processes such as $e^+e^- \leftrightarrow N\bar{N}$ or $N^{(*)} \to Ne^+e^-$. The latter is an important tool to probe the initial stages of heavy-ion collisions when forming a quark-gluon plasma, since dileptons (e^+e^- or $\mu^+\mu^-$ pairs) escape the interaction zone mostly unharmed.

- The **axial form factors** of the nucleon can be probed by the weak interaction using W and Z bosons. Examples are neutrino scattering off the nucleon, or the neutron beta decay which is the process $n \to pe^-\bar{\nu}_e$. The nucleon's axial charge g_A is a basic ingredient in many low-energy relations.

- The **pseudoscalar form factor** of the nucleon is proportional to the $N\pi$ coupling, which enters in the NN interaction through pion exchange.

- The nucleon's **scalar form factor** is not directly measurable but related to the derivative dM/dm_q of the nucleon mass with respect to the current-quark mass (the so-called nucleon **sigma term**) by the **Feynman-Hellmann theorem**. In addition, the Higgs boson could couple to the nucleon through a top-quark loop.

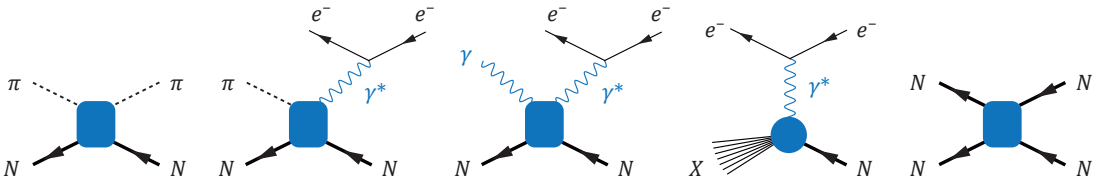

FIG. 4.16: Experimental processes involving nucleons, pions and photons.

On the one hand, measuring form factors gives us experimental information on the internal quark-gluon structure of the probed hadrons and their resonances. On the other hand, these basic quantities appear as building blocks in other scattering processes (Fig. 4.16), which are experimentally accessible but theoretically more complicated:

- ***Nπ* scattering** has been the traditional tool for extracting nucleon resonances. The scattering amplitude has resonance poles, $N\pi \to N^* \to N\pi$, whose residues are the $NN^*\pi$ coupling strengths. Historically, the nucleon resonances have been named after the incoming partial wave $L_{2I,2J}$ in $N\pi$ scattering, with $L = S, P, D, F, \ldots$: the Roper resonance is P_{11}, the $N(1535)$ is S_{11}, etc. Because many of the higher-lying excitations predicted by the quark model have not been seen in $N\pi$ scattering, a common assumption has been that they may not couple strongly to $N\pi$.

- **Meson electroproduction** is the process $N\gamma^* \to NM$, where the virtual photon is produced by the electron and M is the meson. In **photoproduction** the photon is real. These reactions also create nucleon resonances but involve their electromagnetic transition form factors. Thus, if some resonance couples weakly to $N\pi$ but has a large electromagnetic coupling, it should be easier to detect in this way. Combined with improved partial-wave analyses, photo- and electroproduction experiments have indeed found new baryon resonances in recent years. A typical question here concerns the separation of the resonance contributions (like $N\gamma^* \to N^* \to NM$) from the quantum-field theoretical 'background'.

- **Compton scattering** is the process where two photons couple to the nucleon, each of which can be real or virtual. It encodes the nucleon's polarizabilities, which describe the nucleon's response to an external electromagnetic field, but also structure functions and generalized parton distributions (GPDs).

- In **deep inelastic scattering (DIS)** the nucleon is broken up by the highly virtual photon and one measures the inclusive cross section $eN \to eX$. DIS encodes the nucleon's structure functions, which give us access to the partonic structure of the nucleon and its parton distribution functions (PDFs). The early DIS measurements in the 1960s/70s have provided first convincing evidence for the existence of quarks.

- Finally, ***NN* scattering** is the elementary reaction in nucleus-nucleus and heavy-ion collisions which are performed e.g. at the LHC and RHIC. The NN interaction is also the basic ingredient in nuclear physics, and in contrast to its long-range part which is mediated by pion exchange, the short-range nuclear force is still not well understood.

Even though this list only contains processes involving the nucleon, the discussion should make it clear that a good understanding of reactions with baryons and mesons, and the various couplings and form factors they contain, is essential for many questions in hadron physics, among them hadron spectroscopy.

A general matrix element can be written as

$$\langle p_1' \dots p_n' \,|\, \mathsf{T}\, j^\Gamma(x) \dots |\, p_1 \dots p_n \rangle \,, \tag{4.5.1}$$

where $\{p_i\}$ and $\{p_i'\}$ are the onshell momenta of the incoming and outgoing particles. The legs associated with the currents (if there are any) are offshell, i.e., their squared momentum is not fixed but arbitrary. After splitting off the spinors u_α, $\bar{u}_\alpha$ for onshell spin-$\frac{1}{2}$ particles, or polarization vectors ε^μ for spin-1 particles etc., the remainder can be expanded in a tensor basis:

$$\mathcal{M}^{\mu\nu\dots}_{\alpha\beta\dots}(p_1' \dots p_n) = \sum_{i=1}^{N} F_i(\dots)\, \tau_i(p_1' \dots p_n)^{\mu\nu\dots}_{\alpha\beta\dots} \,, \tag{4.5.2}$$

where the Lorentz-invariant amplitudes or form factors $F_i(\dots)$ are analytic functions of the invariant momentum variables and carry the information on the process.

Kinematic variables. Let us work out the kinematics for a generic scattering process shown in Fig. 4.17,

$$A(p_i) + B(k_i) \to A'(p_f) + B'(k_f), \tag{4.5.3}$$

where the incoming and outgoing states are not necessarily on their mass shells. If all particles are onshell, then the process describes e.g. eN scattering, $N\pi$ scattering or NN scattering in Figs. (4.15–4.16). If k_i is offshell, it corresponds to meson electroproduction or virtual Compton scattering, and if also k_f is offshell, doubly-virtual Compton scattering. An example where only p_f is offshell is inelastic eN scattering, where p_f is the total momentum of the decay products.

Let us express the amplitude in terms of three independent momenta

$$p = \frac{p_i + p_f}{2} \,, \qquad k = \frac{k_i + k_f}{2} \,, \qquad q = p_f - p_i = k_i - k_f \,, \tag{4.5.4}$$

where p and k are the average momenta of A and B, respectively, and q is the momentum transfer, with the inverse relations

$$\begin{aligned} p_i &= p - \tfrac{q}{2} \,, & k_i &= k + \tfrac{q}{2} \,, \\ p_f &= p + \tfrac{q}{2} \,, & k_f &= k - \tfrac{q}{2} \,. \end{aligned} \tag{4.5.5}$$

The amplitudes $F_i(\dots)$ can then depend on six Lorentz invariants p^2, k^2, q^2, $p\cdot k$, $p\cdot q$ and $k\cdot q$. It is convenient to define the **Mandelstam variables** s, u and t,

$$\begin{aligned} s &= (p_i + k_i)^2 = (p_f + k_f)^2 = (p + k)^2, \\ u &= (p_i - k_f)^2 = (p_f - k_i)^2 = (p - k)^2, \\ t &= (p_f - p_i)^2 = (k_i - k_f)^2 = q^2 \,, \end{aligned} \tag{4.5.6}$$

whose sum is

$$s + t + u = 2p^2 + 2k^2 + q^2 = p_i^2 + p_f^2 + k_i^2 + k_f^2 \,. \tag{4.5.7}$$

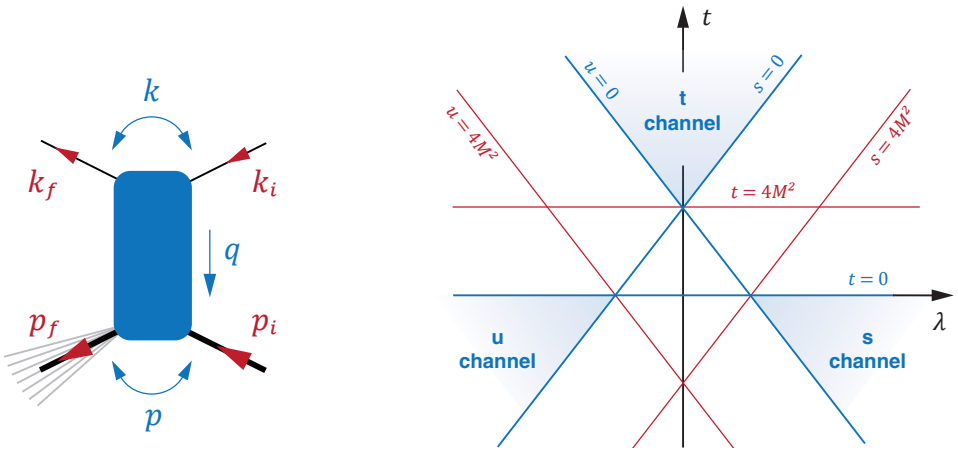

FIG. 4.17: Kinematics in $2 \to 2$ scattering and Mandelstam plane for identical masses.

If we write $p_i^2 = M^2$, $k_i^2 = m^2$, $p_f^2 = M'^2$ and $k_f^2 = m'^2$, then the six independent variables are given by

$$t = q^2\,, \qquad \lambda = \frac{p\cdot k}{M^2} = \frac{s-u}{4M^2}\,, \tag{4.5.8}$$

where we defined the **crossing variable** λ, and

$$\frac{p^2+k^2}{2} = \frac{M^2+M'^2+m^2+m'^2-q^2}{4} = \frac{s+u}{4}\,, \qquad \omega = \frac{p\cdot q}{2M^2} = \frac{M'^2-M^2}{4M^2}\,,$$
$$\frac{p^2-k^2}{2} = \frac{M^2+M'^2-m^2-m'^2}{4}\,, \qquad \omega' = \frac{k\cdot q}{2M^2} = \frac{m^2-m'^2}{4M^2}\,.$$

For one-particle exchanges in the t channel like in Fig. 4.15, t is the squared momentum of the exchange particle and it is common to define the momentum transfer variable

$$\tau = -\frac{q^2}{4M^2} = \frac{Q^2}{4M^2}\,. \tag{4.5.9}$$

In a $2 \to 2$ scattering process where all particles are onshell and their masses are fixed, only t and λ remain independent. They define the **Mandelstam plane**, where the physical regions of the process and its singularity structure can be visualized. The s, t and u-channel processes correspond to

$$\begin{aligned} s\text{ channel}: &\quad 1+2 \to 3+4\,,\\ t\text{ channel}: &\quad 1+\bar{3} \to \bar{2}+4\,,\\ u\text{ channel}: &\quad 1+\bar{4} \to \bar{2}+3\,, \end{aligned} \tag{4.5.10}$$

where e.g. $\bar{3}$ is the antiparticle of 3 with opposite momentum. Crossing symmetry implies that all these processes are described by the same amplitudes $F_i(s,t,u)$ but with different physical domains on the Mandelstam plane. In the s-channel reaction, $s > (M+m)^2$ is the square of the total energy in the center-of-mass (CM) frame and t

is the momentum transfer. In the t and u-channel processes, these roles are exchanged. For example, in $N\pi$ scattering the three processes are

$$\begin{aligned} s \text{ channel}: &\quad N(p_i) + \pi^+(k_i) \to N(p_f) + \pi^+(k_f)\,, \\ t \text{ channel}: &\quad N(p_i) + \bar{N}(-p_f) \to \pi^-(-k_i) + \pi^+(k_f)\,, \\ u \text{ channel}: &\quad N(p_i) + \pi^-(-k_f) \to \pi^-(-k_i) + N(p_f)\,, \end{aligned} \tag{4.5.11}$$

where the s, u channels correspond to $N\pi$ scattering and the t channel to $N\bar{N} \leftrightarrow \pi^+\pi^-$ annihilation. In this case the amplitude is symmetric under $s \leftrightarrow u$ crossing and therefore the F_i can only depend on t and λ^2.

In general, the physical regions in the Mandelstam plane are determined by the **Kibble function**

$$\Phi = stu - \frac{as + bt + cu}{M^2 + M'^2 + m^2 + m'^2} \geq 0\,, \tag{4.5.12}$$

where

$$\begin{aligned} a &= (M^2 m^2 - M'^2 m'^2)(M^2 + m^2 - M'^2 - m'^2)\,, \\ b &= (M^2 M'^2 - m^2 m'^2)(M^2 - m^2 + M'^2 - m'^2)\,, \\ c &= (M^2 m'^2 - M'^2 m^2)(M^2 - m^2 - M'^2 + m'^2)\,. \end{aligned} \tag{4.5.13}$$

For an elastic scattering process with $M = M'$ and $m = m'$, this reduces to $a = c = 0$ and therefore

$$\Phi = t\left[su - (M^2 - m^2)^2\right] \geq 0\,. \tag{4.5.14}$$

The simplest case where all masses are equal and therefore $stu \geq 0$ is shown in Fig. 4.17. Examples for such processes are $\pi\pi$ or NN scattering. The natural variables to describe the physical s-channel region ($s \geq 0$, $t \leq 0$, $u \leq 0$) are then the Mandelstam variable $s \geq 4M^2$ and the angular variable $z = \cos\theta_{\rm CM}$ with $-1 \leq z \leq 1$, where $\theta_{\rm CM}$ is the scattering angle in the CM frame, see Eq. (4.5.26). Forward scattering ($\theta_{\rm CM} = 0$) corresponds to $t = 0$ and backward scattering ($\theta_{\rm CM} = \pi$) to $u = 0$. Employing Legendre polynomials $P_l(z)$, one can perform a **partial-wave expansion** of the amplitude:

$$F(s,z) = \sum_{l=0}^{\infty} (2l+1)\, F_l(s)\, P_l(z)\,. \tag{4.5.15}$$

The Mandelstam plane is particularly useful for studying the analytic structure of the amplitudes. Analyticity means that the scattering amplitudes are analytic functions of s, t and u regarded as complex variables. Their only singularities are those imposed by unitarity, which are simple poles due to the exchange of physical particles and branch cuts due to intermediate multiparticle states. For example, if the s-channel process in Fig. 4.17 generates a bound state below the two-particle threshold, it will show up as a pole at some constant $s < 4M^2$ which is a line in the Mandelstam plane. A resonance above threshold will form another line of constant s, however with a pole on a higher Riemann sheet that can at best produce a bump in the partial wave $F_i(s)$. If the amplitude is crossing-symmetric in $s \leftrightarrow u$, the same singularity structure in the u channel appears through lines of constant u. If the t-channel process produces bound states and resonances, they will form lines of constant t. Thus, the angular dependence of the amplitude at fixed s will be influenced by singularities in crossed channels.

In **deep inelastic scattering** $eN \to eX$, $m = m'$ is the electron mass and M the nucleon mass, whereas $W = M'$ is the total invariant mass of the particles in the final state X, which is not fixed (also called the 'missing mass'). The process is described by the three variables $\{s,t,u\}$ or, equivalently, τ, λ and any of the variables

$$\omega = \frac{W^2 - M^2}{4M^2}\,, \quad \nu = \frac{p_i \cdot q}{M} = 2M\,(\tau + \omega)\,, \quad x = -\frac{q^2}{2M\nu} = \frac{\tau}{\tau + \omega}\,. \tag{4.5.16}$$

With $W \geq M$, the **Bjorken variable** $0 < x \leq 1$ reduces to $x = 1$ for elastic scattering. In Sec. 5.1 we will see that for a one-photon exchange interaction the hadronic part $\gamma^* N \to X$ does not depend on λ but only on τ and ω. It is parametrized by the nucleon's **structure functions**, which are usually expressed in terms of $\{\tau, x\}$ or $\{\nu, x\}$.

Finally, in processes such as Compton scattering or photo- and electroproduction, the onshell nucleon has mass $M = M'$ whereas m^2 or m'^2 (or both of them) can be virtual. The amplitude then depends on four variables, for example $\{s,t,u,\omega'\}$ or $\{\tau,\lambda,m^2,m'^2\}$, where ω' is related to the 'skewness' variable.

So far we have not specified any Lorentz frame because the above variables are Lorentz-invariant. Their interpretation in terms of energies and a scattering angle, however, depends on the reference frame. In the following we work out the kinematics in the center-of mass and laboratory frames.

■ In the s-channel **center-of-mass (CM) frame** the spatial component of the total momentum $p_i + k_i = p_f + k_f$ vanishes:

$$p_i = \begin{pmatrix} \varepsilon \\ \boldsymbol{k} \end{pmatrix}, \qquad k_i = \begin{pmatrix} E \\ -\boldsymbol{k} \end{pmatrix}, \qquad p_f = \begin{pmatrix} \varepsilon' \\ \boldsymbol{k}' \end{pmatrix}, \qquad k_f = \begin{pmatrix} E' \\ -\boldsymbol{k}' \end{pmatrix}. \tag{4.5.17}$$

For fixed masses, only two of the variables in (4.5.17) are independent, for example the CM momentum $|\boldsymbol{k}|$ and the scattering angle defined by $\boldsymbol{k}\cdot\boldsymbol{k}' = |\boldsymbol{k}||\boldsymbol{k}'|\cos\theta_{\rm CM}$, which can be related to the Mandelstam variables s and t. The variable $s = (p_i + k_i)^2 = (\varepsilon + E)^2 = (\varepsilon' + E')^2$ is the total CM energy squared. From the mass-shell conditions one can express all energies in terms of s,

$$\varepsilon = \frac{s + M^2 - m^2}{2\sqrt{s}}\,, \quad E = \frac{s - M^2 + m^2}{2\sqrt{s}}\,, \quad \varepsilon' = \frac{s + M'^2 - m'^2}{2\sqrt{s}}\,, \quad E' = \frac{s - M'^2 + m'^2}{2\sqrt{s}} \tag{4.5.18}$$

as well as the three-momenta:

$$\begin{aligned} \boldsymbol{k}^2 &= \varepsilon^2 - M^2 = E^2 - m^2 = \frac{\left[s - (M+m)^2\right]\left[s - (M-m)^2\right]}{4s} = \frac{\bar\lambda(s, M^2, m^2)}{4s}\,, \\ \boldsymbol{k}'^2 &= \varepsilon'^2 - M'^2 = E'^2 - m'^2 = \frac{\left[s - (M'+m')^2\right]\left[s - (M'-m')^2\right]}{4s} = \frac{\bar\lambda(s, M'^2, m'^2)}{4s}\,. \end{aligned} \tag{4.5.19}$$

The **triangle function** $\bar\lambda(x,y,z)$ is defined as

$$\bar\lambda(x,y,z) = x^2 + y^2 + z^2 - 2xy - 2yz - 2xz \tag{4.5.20}$$

and invariant under permutation of its arguments. The variable t is given by

$$t = (p_i - p_f)^2 = (\varepsilon - \varepsilon')^2 - (\boldsymbol{k} - \boldsymbol{k}')^2 = M^2 + M'^2 - 2\varepsilon\varepsilon' + 2|\boldsymbol{k}||\boldsymbol{k}'|\cos\theta_{\rm CM}\,, \tag{4.5.21}$$

from where one can relate the scattering angle to s and t:

$$\cos\theta_{\rm CM} = \frac{s^2 + 2st - s(M^2 + M'^2 + m^2 + m'^2) + (M^2 - m^2)(M'^2 - m'^2)}{\sqrt{\bar\lambda(s, M^2, m^2)\,\bar\lambda(s, M'^2, m'^2)}}\,. \tag{4.5.22}$$

For **elastic scattering** with $M = M'$, $m = m'$ these relations simplify to $\varepsilon = \varepsilon'$, $E = E'$, $\boldsymbol{k}^2 = \boldsymbol{k}'^2$,

$$\cos\theta_{\rm CM} = 1 + \frac{2st}{\bar\lambda(s, M^2, m^2)}\,, \qquad \bar\lambda(s, M^2, m^2) = (s - M^2 - m^2)^2 - 4M^2m^2 \tag{4.5.23}$$

and the Mandelstam variables in terms of $\boldsymbol{k}^2$ and $\cos\theta_{\rm CM}$ become

$$\begin{aligned} s &= \left(\sqrt{\boldsymbol{k}^2+M^2}+\sqrt{\boldsymbol{k}^2+m^2}\right)^2 , \\ t &= -2\boldsymbol{k}^2\,(1-\cos\theta_{\rm CM})\,, \\ u &= -2\boldsymbol{k}^2\,(1+\cos\theta_{\rm CM}) + \left(\sqrt{\boldsymbol{k}^2+M^2}-\sqrt{\boldsymbol{k}^2+m^2}\right)^2 . \end{aligned} \tag{4.5.24}$$

If all masses are equal ($m = M$), we obtain

$$\varepsilon = E = \frac{\sqrt{s}}{2}\,, \quad \boldsymbol{k}^2 = \frac{s-4M^2}{4}\,, \quad \cos\theta_{\rm CM} = 1+\frac{2t}{s-4M^2}\,, \quad \bar\lambda(s,M^2,M^2) = s\,(s-4M^2) \tag{4.5.25}$$

and the Mandelstam variables become

$$s = 4\,(\boldsymbol{k}^2+M^2)\,, \quad t = -2\boldsymbol{k}^2\,(1-\cos\theta_{\rm CM})\,, \quad u = -2\boldsymbol{k}^2\,(1+\cos\theta_{\rm CM})\,. \tag{4.5.26}$$

Here, forward scattering ($\theta_{\rm CM} = 0$) corresponds to $t = 0$ and backward scattering ($\theta_{\rm CM} = \pi$) to $u = 0$.

■ Next, we consider the **lab frame** where p_i is at rest:

$$p_i = \begin{pmatrix} M \\ \boldsymbol{0} \end{pmatrix}, \qquad k_i = \begin{pmatrix} E \\ \boldsymbol{k} \end{pmatrix}, \qquad p_f = \begin{pmatrix} \varepsilon' \\ \boldsymbol{p}' \end{pmatrix}, \qquad k_f = \begin{pmatrix} E' \\ \boldsymbol{k}' \end{pmatrix}. \tag{4.5.27}$$

We use the same symbols E, E', ε, $\boldsymbol{k}$ and $\boldsymbol{k}'$ as before, but keep in mind that these quantities are not the same as in Eq. (4.5.17) since they are the energies and three-momenta in the lab frame. The scattering angle in the lab frame is defined by $\boldsymbol{k}\cdot\boldsymbol{k}' = |\boldsymbol{k}||\boldsymbol{k}'|\cos\theta$. In this case we have

$$\begin{aligned} s &= (p_i+k_i)^2 = (M+E)^2 - \boldsymbol{k}^2 = M^2+m^2+2ME\,, \\ t &= (p_f-p_i)^2 = (\varepsilon'-M)^2 - \boldsymbol{p}'^2 = M^2+M'^2-2M\varepsilon'\,, \\ u &= (p_i-k_f)^2 = (M-E')^2 - \boldsymbol{k}'^2 = M^2+m'^2-2ME'\,, \end{aligned} \tag{4.5.28}$$

from where we can relate the energies to the Mandelstam variables:

$$E = \frac{s-M^2-m^2}{2M}\,, \qquad E' = \frac{M^2+m'^2-u}{2M}\,, \qquad \varepsilon' = \frac{M^2+M'^2-t}{2M}\,. \tag{4.5.29}$$

The three-momenta are then given by

$$\begin{aligned} \boldsymbol{k}^2 &= E^2-m^2 = \frac{\bar\lambda(s,M^2,m^2)}{4M^2}\,, \\ \boldsymbol{k}'^2 &= E'^2-m'^2 = \frac{\bar\lambda(u,M^2,m'^2)}{4M^2}\,, \\ \boldsymbol{p}'^2 &= \varepsilon'^2-M'^2 = \frac{\bar\lambda(t,M^2,M'^2)}{4M^2}\,. \end{aligned} \tag{4.5.30}$$

The Mandelstam variables are related by $s+t+u = M^2+M'^2+m^2+m'^2$. The scattering angle in the lab frame can be worked out using

$$t = (k_i-k_f)^2 = (E-E')^2 - (\boldsymbol{k}-\boldsymbol{k}')^2 = m^2+m'^2-2EE'+2|\boldsymbol{k}||\boldsymbol{k}'|\cos\theta\,, \tag{4.5.31}$$

from where we obtain

$$\cos\theta = \frac{2M^2(t-m^2-m'^2)-(s-M^2-m^2)(u-M^2-m'^2)}{\sqrt{\bar\lambda(s,M^2,m^2)\,\bar\lambda(u,M^2,m'^2)}}\,. \tag{4.5.32}$$

■ A practical example for the case $m = m' = 0$ is (elastic or inelastic) ***eN* scattering** with a nucleon mass M and electron mass $m = m' \ll M$. The lab frame is the natural frame for fixed-target experiments, where the experimental control parameters are the initial and final lepton energies E, E' and the scattering angle θ. In this case the above relations become

$$E = |\boldsymbol{k}| = \frac{s-M^2}{2M}\,, \quad E' = |\boldsymbol{k}'| = \frac{M^2-u}{2M}\,, \quad \varepsilon' = \frac{M^2+M'^2-t}{2M}\,, \quad \boldsymbol{p}'^2 = \frac{\lambda(t,M^2,M'^2)}{4M^2}\,, \tag{4.5.33}$$

and the scattering angle is given by

$$\sin^2\frac{\theta}{2}=\frac{1-\cos\theta}{2}=\frac{M^2t}{(s-M^2)(u-M^2)}\,. \tag{4.5.34}$$

Expressing the Mandelstam variables through τ, λ and ω defined in Eqs. (4.5.8–4.5.9),

$$\begin{aligned} s &= M^2\left[1+2\left(\tau+\omega+\lambda\right)\right], \\ u &= M^2\left[1+2\left(\tau+\omega-\lambda\right)\right], \end{aligned} \qquad t=-4M^2\tau \tag{4.5.35}$$

we find

$$\begin{aligned} E &= M\left(\lambda+\tau+\omega\right), \\ E' &= M\left(\lambda-\tau-\omega\right), \end{aligned} \qquad \sin^2\frac{\theta}{2}=\frac{\tau}{\lambda^2-(\tau+\omega)^2}\,. \tag{4.5.36}$$

The condition (4.5.12) for the physical region becomes

$$\Phi=t\left(su-M^2M'^2\right)=-16M^4\,\tau\left[\tau+(\tau+\omega)^2-\lambda^2\right]\geq 0\,. \tag{4.5.37}$$

From the inverse relations

$$\lambda=\frac{E+E'}{2M}\,,\qquad \tau=\frac{EE'}{M^2}\,\sin^2\frac{\theta}{2}\,,\qquad \omega+\tau=\frac{E-E'}{2M} \tag{4.5.38}$$

we see that the crossing variable is proportional to the average lepton energy. The variable ν from Eq. (4.5.16) plays the role of the energy transfer from the electron to the proton, $\nu=E-E'$, and another commonly used variable is

$$y=\frac{p_i\cdot q}{p_i\cdot k_i}=\frac{2\left(\tau+\omega\right)}{\lambda+\tau+\omega-\omega'}=1-\frac{E'}{E}\,, \tag{4.5.39}$$

which becomes the lepton energy loss ($0\leq y\leq 1$) in the lab frame. In the case of elastic scattering ($\omega=0$) there are only two independent variables and we have the additional constraint

$$E'=\frac{E}{1+\frac{2E}{M}\,\sin^2\frac{\theta}{2}}\,. \tag{4.5.40}$$

■ We also work out the **cross section** for eN scattering. The general form of the cross section for $2\to n$-particle scattering has the form

$$d\sigma=\frac{|\mathcal{M}|^2\,d\Phi}{4\sqrt{(p_i\cdot k_i)^2-M^2m^2}}\,, \tag{4.5.41}$$

where $|\mathcal{M}|^2$ is the invariant amplitude, $d\Phi$ is the phase space element and the denominator is the incoming flux factor. For two particles in the final state, the phase space is given by

$$d\Phi=\frac{d^3p_f}{(2\pi)^3\,2\varepsilon'}\,\frac{d^3k_f}{(2\pi)^3\,2E'}\,(2\pi)^4\,\delta^4(p_i+k_i-k_f-p_f)\,, \tag{4.5.42}$$

where p_f and k_f are the outgoing momenta and ε' and E' their energies in the lab frame, cf. (4.5.27). Integration over d^3p_f removes the three-dimensional $\delta-$function for three-momentum conservation. For vanishing electron masses, inserting $d^3k_f=dE'E'^2d\Omega$ yields

$$d\Phi=\frac{d\Omega}{(4\pi)^2}\,\frac{E'}{\varepsilon'}\,dE'\,\delta(M+E-E'-\varepsilon')\,. \tag{4.5.43}$$

We can express the final-state energy by $\varepsilon'=\sqrt{\boldsymbol{q}^2+W^2}=\sqrt{\boldsymbol{q}^2+M^2+4M^2\omega}$, where for elastic scattering the energy-conservation constraint is satisfied for $\omega=0$. Hence, we can rewrite the $\delta-$function in the variable ω:

$$\delta(M+E-E'-\varepsilon')=\frac{\varepsilon'}{2M^2}\,\delta(\omega)\quad\Rightarrow\quad d\Phi=\frac{d\Omega}{(4\pi)^2}\,\frac{E'}{2M^2}\,dE'\,\delta(\omega)\,. \tag{4.5.44}$$

On the other hand, we have

$$\int dE'\,f(E')\,\frac{\delta(\omega)}{2M}=\frac{f(E')}{2M\left|\frac{d\omega}{dE'}\right|_{\omega=0}}\overset{(4.5.38)}{=}\frac{f(E')}{1+\frac{2E}{M}\,\sin^2\frac{\theta}{2}}\bigg|_{\omega=0}\overset{(4.5.40)}{=}f(E')\,\frac{E'}{E}\,. \tag{4.5.45}$$

Combining this with the flux factor $4p_i\cdot k_i=4ME$, we arrive at

$$\frac{d\sigma}{d\Omega}=\frac{1}{4M^2}\,\frac{|\mathcal{M}|^2}{16\pi^2}\,\frac{E'^2}{E^2}\,. \tag{4.5.46}$$

4.5.2 Form factors

We already motivated the basic ideas behind form factors from an experimental point of view in Sec. 4.5.1. When resolving the structure of a hadron using electromagnetic and weak interactions, the elementary structure observables are form factors. Viewed from a distance, the proton looks like a point fermion that only carries a charge and a magnetic moment, but when probed with short-wavelength photons (or other currents) it reveals more and more of its composite nature which is encoded in the momentum dependence of its form factors.

Form factors are encoded in the **current matrix elements**

$$\langle \lambda'(p_f)|\, j_a^\Gamma(0)\, |\lambda(p_i)\rangle\,, \tag{4.5.47}$$

where $|\lambda(p_i)\rangle$ is a one-particle state with onshell momentum p_i and $|\lambda'(p_f)\rangle$ one with momentum p_f. The currents $j_a^\Gamma(x)$ can be any of the quark bilinears in Eq. (3.1.23) such as vector, axialvector, scalar or pseudoscalar currents. On theoretical grounds, a current matrix element can be motivated in several ways:

■ In Eq. (3.1.147) we saw that current matrix elements arise from elementary correlation functions at the pole positions, i.e., they are the residues at the hadronic double pole. This also gives us an intuitive way to understand **elastic** and **transition form factors**: in the second case, the initial and final hadrons can be different and correspond to different poles, provided that the symmetries in the process (e.g. baryon number conservation) are preserved.

■ In Eq. (3.1.141) we found that the contraction of the Bethe-Salpeter wave function with a Dirac-flavor matrix $\Gamma\,\mathsf{t}_a$ gives rise to decay constants $\langle 0|\, j^\Gamma(0)\, |\lambda(p)\rangle$, which are gauge invariant and depend on the onshell momentum p. In the same way, a current matrix element arises from the contraction of the object $\langle \lambda'(p_f)|\, \mathsf{T}\psi_\alpha(x)\, \bar\psi_\beta(y)\, |\lambda(p_i)\rangle$ with open quark and antiquark legs:

$$\begin{aligned} &-(\mathsf{t}_a)_{ji}\,\Gamma_{\beta\alpha}\,\langle \lambda'(p_f)|\, \mathsf{T}\psi_{\alpha i}(x)\, \bar\psi_{\beta j}(x)\, |\lambda(p_i)\rangle \\ &\qquad = \langle \lambda'(p_f)|\, j_a^\Gamma(x)\, |\lambda(p_i)\rangle = \langle \lambda'(p_f)|\, j_a^\Gamma(0)\, |\lambda(p_i)\rangle\, e^{iq\cdot x}\,, \end{aligned} \tag{4.5.48}$$

where $q = p_f - p_i$. Thus, the current couples to the quarks inside the hadrons as shown in Fig. 4.18. The resulting matrix element is again gauge invariant and depends on the two onshell momenta p_f and p_i.

The three-point function depends on two independent momenta, e.g. the incoming and outgoing momenta p_i and p_f, or their combinations $p = (p_i + p_f)/2$ and the momentum transfer $q = p_f - p_i$. For elastic form factors we have $p_i^2 = p_f^2 = M^2$ and therefore

$$\begin{aligned} p_f &= p + \tfrac{q}{2} \\ p_i &= p - \tfrac{q}{2} \end{aligned} \quad\Rightarrow\quad \begin{aligned} p_f^2 &= p^2 + \tfrac{q^2}{4} + p\cdot q \stackrel{!}{=} M^2 \\ p_i^2 &= p^2 + \tfrac{q^2}{4} - p\cdot q \stackrel{!}{=} M^2 \end{aligned} \quad\Rightarrow\quad \begin{aligned} &p\cdot q = 0 \\ &p^2 = M^2 - \tfrac{q^2}{4}\,. \end{aligned} \tag{4.5.49}$$

Thus, the only independent variable is the squared momentum transfer q^2. Because $q^2 < 0$ is spacelike in $s-$channel processes such as eN scattering, we work with the spacelike momentum transfer $Q^2 = -q^2$ or equivalently $\tau = Q^2/(4M^2)$.

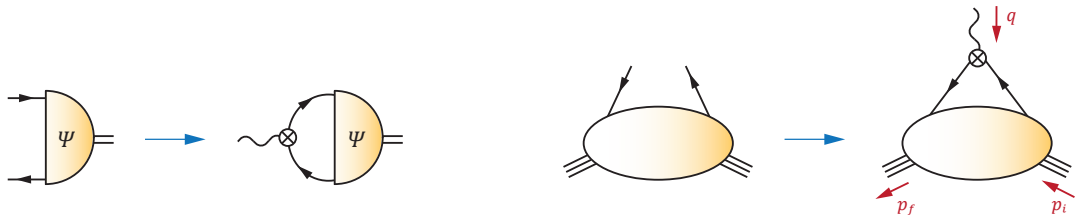

FIG. 4.18: Current matrix element of a hadron, viewed as the Dirac-flavor contraction of the four-point function in Eq. (4.5.48) in analogy to the Bethe-Salpeter wave function.

Form factors. As a specific case of Eq. (4.5.2), form factors are the Lorentz-invariant coefficients of current matrix elements. As an example, consider a spin-$\frac{1}{2}$ particle and a vector current $V^\mu = \bar\psi\gamma^\mu\psi$. In this case, the general decomposition involves the **Dirac** and **Pauli form factors** $F_1(q^2)$ and $F_2(q^2)$:

$$\langle p_f, s'|\, V^\mu(0)\, |p_i, s\rangle = \bar u_{s'}(p_f)\left[\gamma^\mu F_1(q^2) + \sigma^{\mu\nu}\,\frac{iq_\nu}{2M}\,F_2(q^2)\right] u_s(p_i)\,. \tag{4.5.50}$$

Here $\sigma^{\mu\nu} = \frac{i}{2}\,[\gamma^\mu,\gamma^\nu]$ and $u_s(p_i)$, $\bar u_{s'}(p_f)$ are the onshell Dirac spinors with normalization $\bar u_{s'}(p)\,u_s(p) = 2M\,\delta_{ss'}$. The dimensionless form factors depend only on q^2. For two flavors, the **isoscalar** and **isovector** form factors correspond to the currents

$$\begin{aligned} V^\mu &= \bar\psi\gamma^\mu\psi = \bar u\gamma^\mu u + \bar d\gamma^\mu d\,,\\ V_3^\mu &= \bar\psi\,\gamma^\mu\,\mathtt{t}_3\,\psi = \tfrac{1}{2}\,(\bar u\gamma^\mu u - \bar d\gamma^\mu d) \end{aligned} \tag{4.5.51}$$

and the **electromagnetic form factors**, which are linear combinations of them, to the electromagnetic current $V^\mu_{\rm em}$ from Eq. (3.1.92) with the quark charge matrix

$$\mathsf{Q} = \begin{pmatrix} q_u & 0\\ 0 & q_d\end{pmatrix} = \frac{\mathbb{1}}{6} + \frac{\tau_3}{2}\,. \tag{4.5.52}$$

Why are there just *two* form factors in Eq. (4.5.50)? Consider the most generic form of a vector-spinor three-point function $\Omega^\mu(p,q)$. Poincaré covariance and parity invariance in principle allows for 12 tensor structures, for example

$$\{\gamma^\mu,\, p^\mu,\, q^\mu\} \times \{\mathbb{1},\, \not p,\, \not q,\, [\not p, \not q]\} \tag{4.5.53}$$

or linear combinations of those. After sandwiching between the onshell nucleon spinors $\bar u(p_f)$ and $u(p_i)$, we can use the Dirac equation $(\not p - M)\,u(p) = 0$ to eliminate all slashes:

$$\begin{aligned} \bar u(p_f)\,\not q\,u(p_i) &= \bar u(p_f)\,(\not p_f - \not p_i)\,u(p_i) = 0\,,\\ \bar u(p_f)\,\not p\,u(p_i) &= \bar u(p_f)\,\frac{\not p_f + \not p_i}{2}\,u(p_i) = M\,\bar u(p_f)\,u(p_i)\,,\\ \bar u(p_f)\,[\gamma^\mu, \not q]\,u(p_i) &= 4\,\bar u(p_f)\,(p^\mu - M\gamma^\mu)\,u(p_i)\,, \end{aligned} \tag{4.5.54}$$

where the last relation is the **Gordon identity**. As a result, we are left with γ^μ, p^μ and q^μ only.

In addition, charge conjugation imposes the condition

$$C\,\Omega^\mu(-p,q)^T C^T \stackrel{!}{=} -\Omega^\mu(p,q)\,, \tag{4.5.55}$$

where $C = i\gamma^2\gamma^0$ is the charge-conjugation matrix. This is satisfied for γ^μ and p^μ but not for q^μ, which has opposite $C-$parity. To restore it, we would need to attach a factor $p\cdot q$ so that $(p\cdot q)\,q^\mu$ becomes the third basis element, but $p\cdot q = 0$ because the nucleon is onshell, cf. Eq. (4.5.49). Hence, a vector current matrix element can only depend on γ^μ and p^μ. Finally, we use the Gordon identity to express p^μ in terms of γ^μ and $\sigma^{\mu\nu}q_\nu = \frac{i}{2}[\gamma^\mu, \not{q}]$, which leads to the form in (4.5.50).

The same principles can be used to establish the matrix elements of an axialvector current $A^\mu(0)$, a pseudoscalar density $P(0)$ and a scalar density $S(0)$. In these cases, the bracket in (4.5.50) must be replaced with

$$\gamma^\mu\gamma_5\,G_A(q^2) + \gamma_5\,\frac{q^\mu}{2M}\,G_P(q^2)\,, \qquad G_5(q^2)\,i\gamma_5\,, \qquad G_S(q^2)\,, \tag{4.5.56}$$

respectively. $G_A(q^2)$ is the **axial form factor** and $G_P(q^2)$ the 'induced' pseudoscalar form factor of a spin-1/2 baryon. In the limit $q^2 \to 0$, the axial form factor becomes the **axial charge** $g_A = G_A(0)$, whose experimental value $g_A \approx 1.27$ for the nucleon is known from neutron beta decay. $G_5(q^2)$ and $G_S(q^2)$ are the pseudoscalar and scalar form factors.

One can also write down current matrix elements for baryons with higher spin (e.g. for $J = 3/2$ the Dirac spinors must be replaced by **Rarita-Schwinger spinors**), which produces more tensors and thus more form factors, or transition matrix elements between baryons with different spins, or meson form factors, etc.

Current conservation. Next, we want to work out the implications of current conservation for the matrix elements. Vector current conservation $\partial_\mu V^\mu = 0$ implies

$$\partial_\mu \langle\lambda'|\,V^\mu(x)\,|\lambda\rangle = \langle\lambda'|\,V^\mu(0)\,|\lambda\rangle\,\partial_\mu\,e^{iq\cdot x} = iq_\mu\,\langle\lambda'|\,V^\mu(0)\,|\lambda\rangle\,e^{iq\cdot x} \stackrel{!}{=} 0\,, \tag{4.5.57}$$

which means that the vector current matrix element must be transverse with respect to the momentum transfer q_μ. Eq. (4.5.50) already satisfies that constraint because $\sigma^{\mu\nu}q_\mu q_\nu = 0$ and $\bar u(p_f)\not{q}\,u(p_i) = 0$, so this does not impose any constraints on the Dirac and Pauli form factors.

In the axialvector case, the PCAC relation $\partial_\mu A^\mu = 2mP$ tells us that

$$\partial_\mu \langle\lambda'|\,A^\mu(x)\,|\lambda\rangle = iq_\mu\,\langle\lambda'|\,A^\mu(0)\,|\lambda\rangle\,e^{iq\cdot x} \stackrel{!}{=} 2m\,\langle\lambda'|\,P(0)\,|\lambda\rangle\,e^{iq\cdot x}\,. \tag{4.5.58}$$

Inserted into the matrix elements and using Eq. (4.5.56), this entails

$$\cdots\left[i\not{q}\gamma_5\,G_A(q^2) + i\gamma_5\,\frac{q^2}{2M}\,G_P(q^2)\right]\cdots = \cdots\left[2m\,G_5(q^2)\,i\gamma_5\right]\cdots \tag{4.5.59}$$

and with $\not{q}\gamma_5 = \not{p}_f\gamma_5 + \gamma_5\not{p}_i \cong 2M\gamma_5$ using the Dirac equation, we find that the axial and pseudoscalar form factors are related:

$$G_A(q^2) + \frac{q^2}{4M^2}\,G_P(q^2) \stackrel{!}{=} \frac{m}{M}\,G_5(q^2)\,. \tag{4.5.60}$$

It appears that g_A should vanish in the chiral limit $m \to 0$, but this is not the case because the pseudoscalar form factor contains pion poles. The four-point function in Fig. 4.18 must develop meson poles in the t channel for $q^2 = m_\lambda^2$, since $N\bar{N}$ and $q\bar{q}$ are compatible with meson quantum numbers. According to Eq. (3.1.121), the residue involving the $q\bar{q}$ pair is the Bethe-Salpeter wave function of the respective meson and the residue on the $N\bar{N}$ pair is the nucleon-meson coupling constant. Contracted with γ_5, this only leaves pseudoscalar-meson poles whose residues r_λ we defined in Eq. (3.1.142). Thus, at the pion pole $G_5(q^2)$ must have the form

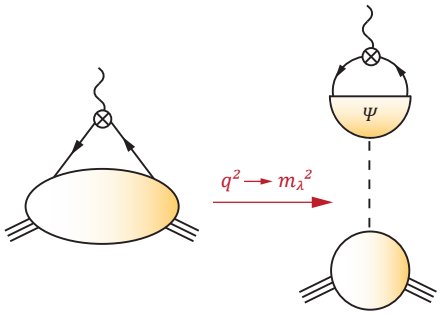

FIG. 4.19: Form factors have meson poles in the t channel.

$$G_5(q^2) = -\frac{2r_\pi}{q^2 - m_\pi^2}\, G_{\pi NN}(q^2) \overset{(3.1.143)}{=} -\frac{m_\pi^2}{q^2 - m_\pi^2}\, \frac{f_\pi}{m}\, G_{\pi NN}(q^2)\,, \tag{4.5.61}$$

which is illustrated in Fig. 4.19. Here we defined an effective pion-nucleon form factor $G_{\pi NN}(q^2)$, which absorbs all further pseudoscalar pole contributions and non-resonant terms and reduces to the pion-nucleon coupling constant $G_{\pi NN}(q^2 = m_\pi^2) = g_{\pi NN}$ at the pion pole. The factor 2 accounts for $G_5\, \mathtt{t}_a \sim 2\, G_{\pi NN}\, \mathtt{t}_a = G_{\pi NN}\, \tau_a$ and the minus sign makes $G_5(q^2 < 0)$ positive. Combined with Eq. (4.5.60), we arrive at the **Goldberger-Treiman relation**

$$g_A = \frac{f_\pi}{M}\, G_{\pi NN}(0) \xrightarrow{\text{chiral limit}} \frac{f_\pi}{M}\, g_{\pi NN}\,, \tag{4.5.62}$$

which connects the nucleon's axial charge with the pion-nucleon coupling. $G_{\pi NN}(0)$ is not measurable in contrast to $g_{\pi NN} \approx 13.2$, which is the residue at the physical pion mass. Together with the experimental values for $f_\pi \approx 92$ MeV, $M \approx 940$ MeV and $g_A \approx 1.27$, the Goldberger-Treiman relation is well realized in nature.

Meson resonances. The appearance of t-channel meson poles in form factors has far-reaching consequences for their analytic structure. Timelike poles appear not only in the pseudoscalar form factor $G_5(q^2)$, but also in

- the Dirac and Pauli vector form factors $F_1(q^2)$ and $F_2(q^2)$, which have 1^{--} vector-meson poles e.g. at $q^2 = m_\rho^2$ or m_ω^2 (depending on the isovector/isoscalar channel) and whose residues are the products of the $\rho/\omega-$nucleon couplings combined with the $\rho/\omega-$meson decay constants;
- the axial form factor $G_A(q^2)$ which has axialvector 1^{++} poles,
- the scalar form factor with scalar poles 0^{++}, etc.

The singularity structure is independent of the hadron because microscopically it originates from the vertex that describes the coupling of the current to the quarks, like the quark-photon vertex discussed in Eq. (3.1.146) in the vector case.

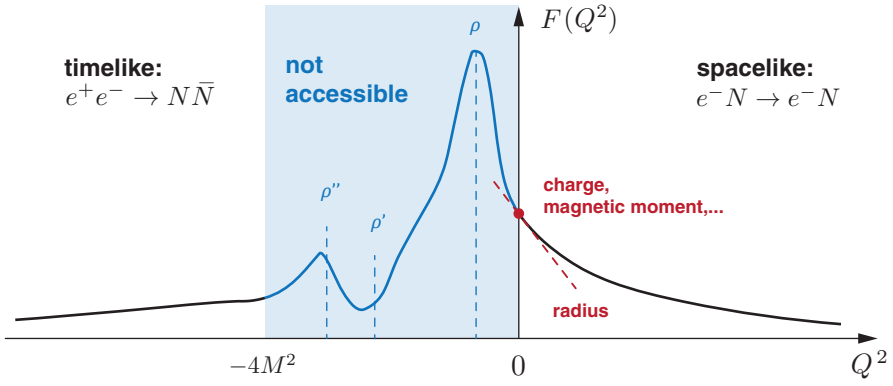

FIG. 4.20: Sketch of a nucleon electromagnetic form factor containing $\rho-$meson bumps. The fictitious curve in the unphysical window is based on the pole structure in the (measured) pion electromagnetic form factor.

In fact, since only the pion is stable with respect to the strong interaction, all other mesons have non-zero hadronic decay widths. Their poles must then move into the complex q^2 plane onto higher Riemann sheets and only produce bumps on the timelike q^2 axis. The respective branch cuts are generated by intermediate multiparticle states containing two pions ($\rho \to \pi\pi$), three pions ($\omega \to \pi\pi\pi$), $K\bar{K}$, etc.

The situation is illustrated in Fig. 4.20 for a generic elastic nucleon vector-isovector form factor with $\rho-$meson bumps. A similar picture with appropriate J^{PC} poles would arise for other types of form factors as well. The form factor's momentum dependence in the spacelike domain ($Q^2 = -q^2 > 0$) can be extracted from elastic electron-nucleon scattering as long as the one-photon exchange process is dominant (more on that below). The timelike region above $p\bar{p}$ production threshold ($q^2 > 4M^2$) can be accessed in e^+e^- annihilation. However, meson resonances should be most pronounced in the window $q^2 \sim 0 \ldots 4$ GeV^2 which is experimentally not accessible; in the deep timelike region the resonance peaks are already washed out. Fortunately, precise data are available for the *pion* electromagnetic form factor which should display a similar resonance structure as in the nucleon case. Here the unphysical window is much smaller ($q^2 = 0 \ldots 4m_\pi^2 \approx 0.08$ GeV^2) and the resonance peaks are indeed directly visible in the data, with a similar shape as in Fig. 4.20.

The timelike resonance structure can be connected with the spacelike behavior of the form factors through **dispersion relations**. Like physical scattering amplitudes, form factors must be analytic everywhere in the complex Q^2 plane except for branch-point singularities starting at $q^2 = 4m_\pi^2$ and extending to infinity, which are due to intermediate two-pion and multiparticle states. The Cauchy formula then tells us that the form factor in the domain of analyticity can be inferred from knowledge of its value on a closed contour, which can be deformed to encompass only the branch cut (see Fig. 4.21). Since the form factor is analytic everywhere else, the difference above and below the branch cut is proportional to its imaginary part, i.e., the discontinuity along the branch cut:

$$F(z_0) = \frac{1}{2\pi i} \oint dz \, \frac{F(z)}{z - z_0} = \frac{1}{\pi} \int\limits_{4m_\pi^2}^{\infty} dz \, \frac{\mathrm{Im}\, F(z)}{z - z_0} \,. \tag{4.5.63}$$

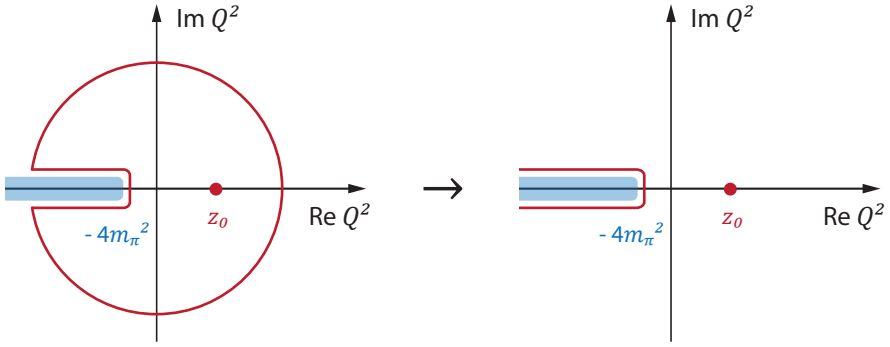

FIG. 4.21: Analytic structure of the form factor $F(Q^2)$ in the complex Q^2 plane and deformation of the integration contour.

Hence, knowledge of the spectral function $\mathrm{Im}\, F(z)$ along the cut is sufficient to determine the spacelike form factor as well. On the other hand, since the experimental knowledge is limited to $q^2 > 4M^2 \sim 4$ GeV^2, one usually has to make assumptions about the timelike behavior to extract such information.

Cross section for elastic eN scattering. The nucleon's electromagnetic form factors in the spacelike region $Q^2 \geq 0$ are experimentally extracted from elastic eN scattering. Since the process is reasonably well described by one-photon exchange, we start from the amplitude (4.1.3) for scattering leptons from a point-like Dirac particle through one-photon exchange (Born approximation):

$$\mathcal{M}_{\sigma\sigma'\lambda\lambda'}(q,p,k) = \frac{e^2}{q^2}\,\bar{u}_{\sigma'}(p_f)\,\gamma^\mu\,u_\sigma(p_i)\,\bar{u}_{\lambda'}(k_f)\,\gamma_\mu\,u_\lambda(k_i)\,. \tag{4.5.64}$$

We worked out the kinematic variables in Eqs. (4.5.4–4.5.9); in particular, since the nucleon and electron scatter elastically, we have $M = M'$, $m = m'$ and therefore

$$p^2 = M^2 - \frac{q^2}{4}\,, \qquad p\cdot q = 0\,, \qquad k^2 = m^2 - \frac{q^2}{4}\,, \qquad k\cdot q = 0 \tag{4.5.65}$$

so that only $\tau = Q^2/(4M^2)$ and $\lambda = p\cdot k/M^2$ remain independent variables. For unpolarized scattering, we take the spin average

$$|\mathcal{M}|^2 = \frac{1}{4}\sum_{\text{spins}} \left|\mathcal{M}\right|^2 = \frac{e^4}{q^4}\,L^{\mu\nu}\,W_{\mu\nu} \tag{4.5.66}$$

which factorizes into a leptonic and a hadronic part. The lepton tensor has the form

$$\begin{aligned} L^{\mu\nu} &= \frac{1}{2}\sum_{\lambda\lambda'} \bar{u}_{\lambda'}(k_f)\gamma^\mu u_\lambda(k_i)\,\bar{u}_\lambda(k_i)\gamma^\nu u_{\lambda'}(k_f) = \\ &= \frac{1}{2}\,\mathrm{Tr}\left[(\not{k}_f + m)\,\gamma^\mu\,(\not{k}_i + m)\,\gamma^\nu\right] \\ &= 2\left(k_f^\mu\,k_i^\nu + k_i^\mu\,k_f^\nu - k_i\cdot k_f\,g^{\mu\nu} + m^2\,g^{\mu\nu}\right) \\ &= 4k^\mu k^\nu - q^\mu q^\nu + 2\left(\frac{q^2}{4} - k^2 + m^2\right)g^{\mu\nu} = 4\left(k^\mu k^\nu + \frac{q^2}{4}T_q^{\mu\nu}\right), \end{aligned} \tag{4.5.67}$$

where in the final step we used the transverse projector

$$T_q^{\mu\nu} = g^{\mu\nu} - \frac{q^\mu q^\nu}{q^2}\,. \tag{4.5.68}$$

Because $k\cdot q = 0$, the lepton tensor is transverse with respect to the photon momentum in both Lorentz indices, which reflects the conservation of the leptonic vector current. For elastic scattering on the hadron side, the hadronic tensor for a structureless fermion has the analogous form

$$\begin{aligned} W^{\mu\nu} &= \frac{1}{2}\sum_{\sigma\sigma'} \bar{u}_{\sigma'}(p_f)\gamma^\mu u_\sigma(p_i)\,\bar{u}_\sigma(p_i)\gamma^\nu u_{\sigma'}(p_f) = \\ &= \frac{1}{2}\,\mathrm{Tr}\left[(\not{p}_f + M)\,\gamma^\mu\,(\not{p}_i + M)\,\gamma^\nu\right] \\ &= 2\left(p_f^\mu p_i^\nu + p_i^\mu p_f^\nu - p_i\cdot p_f\, g^{\mu\nu} + M^2\, g^{\mu\nu}\right) \\ &= 4p^\mu p^\nu - q^\mu q^\nu + 2\left(\frac{q^2}{4} - p^2 + M^2\right) g^{\mu\nu} = 4\left(p^\mu p^\nu + \frac{q^2}{4} T_q^{\mu\nu}\right), \end{aligned} \tag{4.5.69}$$

which is again transverse in both Lorentz indices. Using $T_q^{\mu\nu}\,T_{\mu\nu,q} = 3$ and neglecting the small electron mass, their combination becomes

$$L^{\mu\nu}\,W_{\mu\nu} = 16\left[(p\cdot k)^2 + \frac{q^2}{4}\,(k^2+p^2) + 3\,\frac{q^4}{16}\right] = 16M^4\,(\lambda^2+\tau^2-\tau)\,, \tag{4.5.70}$$

and with $e^2 = 4\pi\alpha$ the result for the invariant squared amplitude is

$$|\mathcal{M}|^2 = \frac{e^4}{q^4}\,L^{\mu\nu}\,W_{\mu\nu} = \frac{16\pi^2\alpha^2}{\tau^2}\,(\lambda^2+\tau^2-\tau)\,. \tag{4.5.71}$$

We already worked out the cross section for elastic eN scattering in Eq. (4.5.46),

$$\frac{d\sigma}{d\Omega} = \frac{1}{4M^2}\,\frac{|\mathcal{M}|^2}{16\pi^2}\,\frac{E'^2}{E^2}\,, \tag{4.5.72}$$

which is expressed through the initial and final lepton energies E, E' in the lab frame. Plugging in the result for $|\mathcal{M}|^2$, the differential cross section becomes

$$\frac{d\sigma}{d\Omega} = \frac{\alpha^2}{4M^2\tau^2}\,\frac{E'^2}{E^2}\,(\lambda^2+\tau^2-\tau) = \underbrace{\frac{\alpha^2\cos^2\frac{\theta}{2}}{4E^2\sin^4\frac{\theta}{2}}\,\frac{E'}{E}}_{\text{Mott}}\left(1 + 2\tau\,\tan^2\frac{\theta}{2}\right), \tag{4.5.73}$$

where we exploited the relations (4.5.36–4.5.38) with $\omega = 0$ to arrive at the second form. The **Mott cross section** describes lepton scattering off a pointlike scalar particle in Born approximation. The parenthesis reflects the nucleon's nature as a spin-$\frac{1}{2}$ particle, which at this point carries no internal structure.

To take the composite nature of the nucleon into account, we must replace the pointlike Dirac current with the general current matrix element

$$\bar{u}(p_f)\gamma^\mu u(p_i) \quad\longrightarrow\quad \bar{u}(p_f)\left(\gamma^\mu F_1(q^2) + \sigma^{\mu\nu}\,\frac{iq_\nu}{2M}\,F_2(q^2)\right)u(p_i) \tag{4.5.74}$$

with Pauli and Dirac form factors F_1 and F_2. Here it is more convenient to work with the **Sachs electric and magnetic form factors**

$$G_E(q^2) = F_1(q^2) - \tau F_1(q^2)\,, \qquad G_M(q^2) = F_1(q^2) + F_2(q^2) \tag{4.5.75}$$

since they do not produce interference terms $\propto F_1 F_2$ in the cross section. The invariant amplitude then becomes

$$|\mathcal{M}|^2 = \frac{16\,\alpha^2\pi^2}{\tau^2}\,\left[\frac{G_E^2 + \tau\,G_M^2}{1+\tau}\,(\lambda^2 - \tau^2 - \tau) + 2\tau^2\,G_M^2\right], \tag{4.5.76}$$

and the resulting cross section is the **Rosenbluth cross section**:

$$\frac{d\sigma}{d\Omega} = \left(\frac{d\sigma}{d\Omega}\right)_{\text{Mott}} \left(\frac{G_E^2 + \tau\,G_M^2}{1+\tau} + 2\tau\,G_M^2\,\tan^2\frac{\theta}{2}\right). \tag{4.5.77}$$

For a structureless fermion ($F_1 = 1$, $F_2 = 0$ or $G_E = G_M = 1$) these formulas reduce to the previous forms (4.5.71) and (4.5.73).

The Rosenbluth cross section allows one to extract the nucleon's electromagnetic form factors under the assumption of one-photon exchange. If we define the kinematic variable

$$\varepsilon = \frac{\lambda^2 - \tau(1+\tau)}{\lambda^2 + \tau(1+\tau)} = \left(1 + 2(1+\tau)\,\tan^2\frac{\theta}{2}\right)^{-1}, \tag{4.5.78}$$

where $\varepsilon = 1$ corresponds to forward scattering and $\varepsilon = 0$ to backward scattering, the cross section takes the form

$$\frac{d\sigma}{d\Omega} = \left(\frac{d\sigma}{d\Omega}\right)_{\text{Mott}} \frac{\varepsilon\,G_E^2 + \tau\,G_M^2}{\varepsilon\,(1+\tau)}\,. \tag{4.5.79}$$

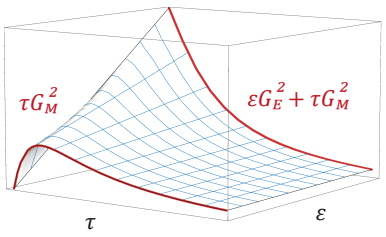

FIG. 4.22: Sketch of the numerator in the Rosenbluth cross section.

Because the form factors only depend on τ, at fixed τ the dependence of the numerator on ε is linear, which allows one to extract the magnetic form factor from the intercept at $\varepsilon = 0$ and the electric form factor from the slope in ε, see Fig. 4.22. This is known as the **Rosenbluth method**. In turn, at large τ (large photon virtualities Q^2) one is less sensitive to G_E and therefore G_E is not so well known at large Q^2. The traditional Rosenbluth results yielded $G_E/G_M \approx const.$ for the proton at large Q^2, which was in agreement with perturbative scaling arguments. However, more recent polarization transfer experiments at Jefferson Lab measured the ratio G_E/G_M directly and found a falloff with Q^2, which even points towards a zero crossing. A likely explanation is that G_E indeed falls off and that the discrepancy is due to **two-photon exchange** effects: although the corresponding diagrams enter with α_{QED}^2 in the cross section, they are large enough to interfere with the extraction of G_E at large Q^2.

The form factors of the proton are directly accessible in $ep \to ep$ scattering, whereas those of the neutron are extracted from scattering on deuterium since there is no free neutron target in nature.

FIG. 4.23: Vertex corrections to the muon-photon vertex which contribute to the muon anomalous magnetic moment. The leading QCD contributions are the hadronic vacuum polarization and hadronic light-by-light scattering diagrams.

Form factor phenomenology. How can we interpret electromagnetic form factors? The Dirac and Pauli form factors at vanishing photon momentum encode the nucleons' charges and their **anomalous magnetic moments**:

$$F_1^p(0) = 1\,, \qquad F_1^n(0) = 0\,, \qquad F_2^p(0) = \kappa_p \approx 1.79\,, \qquad F_2^n(0) = \kappa_n \approx -1.91\,.$$

For the Sachs form factors G_E and G_M this implies

$$G_M^p(0) = \mu_p = 1 + \kappa_p = 2.79\,, \qquad G_M^n(0) = \mu_n = \kappa_n = -1.91\,.$$

The fact that the anomalous magnetic moments differ from zero means that the nucleon is not a pointlike Dirac particle but carries structure. In the analogous case of leptons, the coupling of the photon to an electron or muon has the same form as in Eq. (4.5.50). For pointlike Dirac particles $F_2(0)$ is zero, but due to QED corrections one finds

$$F_2(0) = \frac{\alpha_{\rm QED}}{2\pi} + \cdots \approx 1‰\,. \tag{4.5.80}$$

The leading diagram is the one-loop vertex dressing in Fig. 4.23, followed by higher-order QED corrections. The fact that $F_2(0)$ is much larger for the proton and neutron implies that they are far from pointlike. The **muon** anomalous magnetic moment ('muon $g-2$') is particularly interesting: it has been measured to great precision but there is a current $\sim 4\sigma$ discrepancy between experiment and the Standard Model prediction, which could point towards new physics. Also QCD contributes to this process through the hadronic vacuum polarization (the diagram in Fig. 3.5) and the much smaller hadronic light-by-light scattering diagram. Both of these contributions are tiny compared to the QED effects, but they are almost alone responsible for the theory uncertainty of the Standard Model prediction.

The slopes of the Dirac and Pauli form factors at $Q^2 = 0$ define the Dirac and Pauli **charge radii**:

$$F_1(Q^2) = F_1(0) - \frac{r_1^2}{6}\,Q^2 + \dots\,, \qquad F_2(Q^2) = F_2(0)\left[1 - \frac{r_2^2}{6}\,Q^2 + \dots\right]. \tag{4.5.81}$$

The electric and magnetic charge radii are defined accordingly from G_E and G_M. Also here there has been a surprise in the form of the **proton radius puzzle**: The electric charge radius of the proton measured in muonic hydrogen was found to be significantly smaller ($r_E^p \approx 0.84$ fm) than the previously established CODATA value inferred from ep scattering and hydrogen spectroscopy ($r_E^p \approx 0.88$ fm). Possible explanations include again new physics or two-photon effects, although several new measurements (including ep scattering) tend to agree with the lower radius as well.

Empirically, it turns out that the Sachs form factors can be reasonably well described by a dipole shape over a wide Q^2 range (except for G_E^n which vanishes at the origin). The 'dipole mass' Λ can then be used to estimate the charge radii:

$$G_i(Q^2) \approx \frac{G_i(0)}{(1+Q^2/\Lambda^2)^2}\,, \qquad \Lambda \approx 0.84\,\text{GeV} \quad \Rightarrow \quad r_i \approx \hbar c\,\frac{\sqrt{12}}{\Lambda} \approx 0.8\,\text{fm}\,, \tag{4.5.82}$$

with $\hbar c = 0.197$ GeV fm. Such a dipole behavior for the Sachs form factors agrees with perturbative QCD predictions but has been challenged by measurements of G_E^p/G_M^p at larger Q^2 as mentioned above.

Non-relativistically, form factors can be interpreted as Fourier transforms of charge distributions. Consider the scattering of an electron from a static, spinless source generated by a charge distribution $\rho(\boldsymbol{x})$ that generates the vector potential $A^\mu(\boldsymbol{x})$:

$$\Box A^\mu = j^\mu\,, \qquad A^\mu = \begin{pmatrix} A^0 \\ \mathbf{0} \end{pmatrix}, \qquad j^\mu = \begin{pmatrix} e\rho \\ \mathbf{0} \end{pmatrix}. \tag{4.5.83}$$

The invariant matrix element is given by

$$\mathcal{M} = ie\,\bar{u}(k_f)\gamma^\mu u(k_i)\,\underbrace{\int d^4x\, e^{-iq\cdot x} A_\mu(x)}_{(2\pi)\,\delta(E-E')\,\frac{e}{\boldsymbol{q}^2}\,F(\boldsymbol{q})\,\delta^0_\mu} \tag{4.5.84}$$

which comes about as follows: Because $A^\mu(\boldsymbol{x})$ is time-independent, its Fourier transform in time produces a $\delta-$function $\delta(q^0)$, which enforces $E = E'$ for the lab energies of the incoming and outgoing electron, cf. Eq. (4.5.27). The Maxwell equation $\Box A^\mu = j^\mu$ then reduces to $\Delta A^0 = -e\rho$, and a partial integration yields

$$\int d^3x\, e^{i\boldsymbol{q}\cdot\boldsymbol{x}}\, A^0(\boldsymbol{x}) = \frac{e}{\boldsymbol{q}^2}\int d^3x\, e^{i\boldsymbol{q}\cdot\boldsymbol{x}}\,\rho(\boldsymbol{x}) =: \frac{e}{\boldsymbol{q}^2}\,F(\boldsymbol{q})\,, \tag{4.5.85}$$

where we defined the form factor $F(\boldsymbol{q})$ as the Fourier transformation of the charge density. Therefore, it measures the deviation from the pointlike nature of the source. For a spherically symmetric charge distribution $\rho(\boldsymbol{x}) = \rho(|\boldsymbol{x}|) = \rho(r)$ normalized to $\int d^3x\,\rho(\boldsymbol{x}) = 1$, the form factor at small $|\boldsymbol{q}|$ can be expanded in

$$F(\boldsymbol{q}) = \int d^3x\,\rho(\boldsymbol{x})\left(1 + i\boldsymbol{q}\cdot\boldsymbol{x} - \frac{(\boldsymbol{q}\cdot\boldsymbol{x})^2}{2} + \ldots\right) = 1 - \frac{|\boldsymbol{q}|^2}{6}\,\underbrace{4\pi\int dr\,\rho(r)\,r^4}_{\langle r^2\rangle} + \ldots$$

The coefficient of the quadratic term is the mean-square radius of the 'charge cloud', which motivates the definition of the charge radius in Eq. (4.5.81).

Examples for charge distributions and their corresponding form factors are shown in Fig. 4.24: A pointlike charge corresponds to a constant form factor, an exponential charge distribution to a dipole form factor,

$$\rho(r) = \frac{\Lambda^3}{8\pi}\,e^{-\Lambda r} \quad \Leftrightarrow \quad F(\boldsymbol{q}) = \int d^3x\, e^{i\boldsymbol{q}\cdot\boldsymbol{x}}\,\rho(\boldsymbol{x}) = \frac{1}{(1+|\boldsymbol{q}|^2/\Lambda^2)^2}\,, \tag{4.5.86}$$

a Gaussian to a Gaussian and a homogeneous sphere to an oscillating form factor.

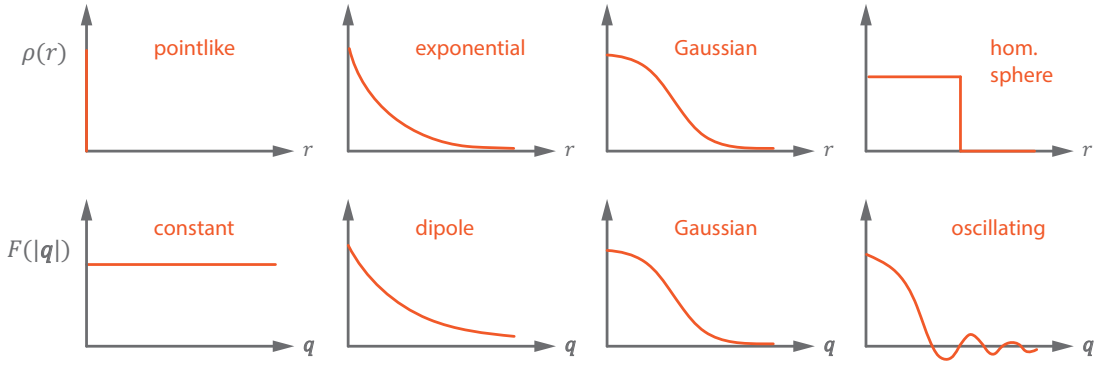

FIG. 4.24: Charge distributions and form factors.

For relativistic nucleons, the interpretation of form factors being Fourier transforms of charge and magnetization distributions has to be taken with a grain of salt. The formulas still look similar to the nonrelativistic case in the **Breit frame**, where the incoming and outgoing proton have opposite momenta ($\boldsymbol{p}_f = -\boldsymbol{p}_i = \boldsymbol{q}/2$) and hence the same energies, so that the photon transfers no energy and $E' = E$; this also implies $Q^2 = -q^2 = |\boldsymbol{q}|^2$. Furthermore, the vector current matrix element in the Breit frame reduces to the form

$$\langle p_f, \sigma' | \, V^0 \, | p_i, \sigma \rangle = 2M \, G_E \, \delta_{\sigma'\sigma} \,, \qquad \langle p_f, \sigma' | \, \boldsymbol{V} \, | p_i, \sigma \rangle = G_M \, \chi^\dagger_{\sigma'} \, i\boldsymbol{\tau} \times \boldsymbol{q} \, \chi_\sigma \,,$$

hence the name 'electric' and 'magnetic' form factors. The charge densities extracted from the experimentally measured G_E^p and G_E^n have shapes shown in Fig. 4.25, which has led to the picture of a neutron behaving like a proton with a positively charged core and a negatively charged **pion cloud**. However, since there is a different Breit frame for each value of Q^2, the relation to charge densities in the lab frame (the rest frame of the nucleon) will suffer from relativistic boost corrections and hence the interpretation of the radii as actual charge and magnetization radii is not directly applicable. In general, while the Lorentz-invariant form factors uniquely specify the electromagnetic structure of a hadron, their physical interpretation in terms of spatial densities depends on the reference frame.

Magnetic moments in the quark model. Current matrix elements encode the complicated nonperturbative substructure of hadrons and have become amenable to first-principle calculations only in recent years. Nevertheless, we can infer simple relations already from the nonrelativistic quark model. We saw in Eq. (3.2.79) that the spin-flavor wave functions for ground-state baryon octet states can be written as the combination of a flavor and a spin doublet:

$$|\lambda\sigma\rangle = \mathcal{D}^\lambda \cdot \mathcal{D}^\sigma = \sum_{m=1}^{2} \mathcal{D}^\lambda_m \, \mathcal{D}^\sigma_m \,, \qquad \lambda \in \{p, n, \Sigma^+, \dots\} \,, \qquad \sigma \in \{\uparrow, \downarrow\}, \qquad (4.5.87)$$

combined with a symmetric spatial wave function and the antisymmetric color part. The flavor doublets $\mathcal{D}^\lambda$ are the flavor wave functions in Table 3.4, and the $SU(2)$ spin doublets $\mathcal{D}^\sigma$ follow if we replace u by $\uparrow$ and d by $\downarrow$. The index m denotes the doublet entries.

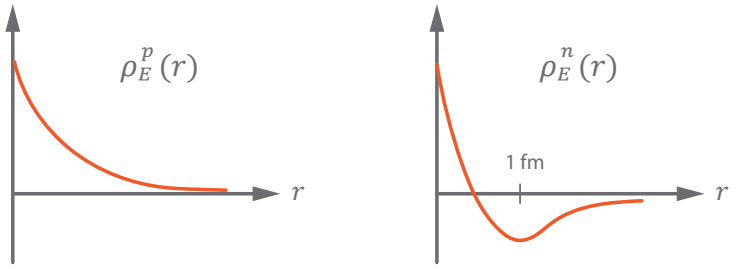

FIG. 4.25: Sketch of the electric charge distributions for proton and neutron in the Breit frame extracted from the measured form factors $G_E^p(Q^2)$ and $G_E^n(Q^2)$.

In the following we are only interested in the spin-flavor part. Its unit normalization is ensured via

$$\langle\lambda'\sigma'|\lambda\sigma\rangle = \frac{1}{\mathcal{N}}\sum_{m'm}\left(\mathcal{D}^{\lambda'}_{m'}\right)^\dagger\left(\mathcal{D}^{\lambda}_{m}\right)\left(\mathcal{D}^{\sigma'}_{m'}\right)^\dagger\left(\mathcal{D}^{\sigma}_{m}\right) \stackrel{!}{=} \delta_{\lambda'\lambda}\,\delta_{\sigma'\sigma}\,, \tag{4.5.88}$$

from where the factor $\mathcal{N}$ has to be determined. From Table 3.4 one can verify

$$\left(\mathcal{D}^{p}_{m'}\right)^\dagger\left(\mathcal{D}^{p}_{m}\right) = \left(\mathcal{D}^{n}_{m'}\right)^\dagger\left(\mathcal{D}^{n}_{m}\right) = \left(\mathcal{D}^{\uparrow}_{m'}\right)^\dagger\left(\mathcal{D}^{\uparrow}_{m}\right) = \delta_{m'm}\,, \tag{4.5.89}$$

e.g. with $u^\dagger u = d^\dagger d = 1$, $u^\dagger d = d^\dagger u = 0$:

$$\left(\mathcal{D}^{p}_{1}\right)^\dagger\left(\mathcal{D}^{p}_{1}\right) = \frac{1}{2}\left(u^\dagger d^\dagger u^\dagger - d^\dagger u^\dagger u^\dagger\right)(udu - duu) = 1\,, \quad \text{etc.} \tag{4.5.90}$$

Inserting this in (4.5.88) yields

$$\langle p\uparrow|p\uparrow\rangle = \langle n\uparrow|n\uparrow\rangle = \frac{1}{\mathcal{N}}\,\mathrm{Tr}\begin{pmatrix}1&0\\0&1\end{pmatrix} = \frac{2}{\mathcal{N}} \quad\Rightarrow\quad \mathcal{N} = 2\,. \tag{4.5.91}$$

The expectation value of a generic flavor (F) and spin (Γ) operator is then

$$\langle\lambda'\sigma'|\,\mathsf{F}\,\Gamma\,|\lambda\sigma\rangle = \frac{3}{\mathcal{N}}\sum_{m'm}\underbrace{\left(\mathcal{D}^{\lambda'}_{m'}\right)^\dagger\mathsf{F}\left(\mathcal{D}^{\lambda}_{m}\right)}_{=:\mathsf{F}^{\lambda'\lambda}_{m'm}}\underbrace{\left(\mathcal{D}^{\sigma'}_{m'}\right)^\dagger\Gamma\left(\mathcal{D}^{\sigma}_{m}\right)}_{=:\Gamma^{\sigma'\sigma}_{m'm}} = \frac{3}{2}\,\mathrm{Tr}\left\{\mathsf{F}^{\lambda'\lambda\,T}\Gamma^{\sigma'\sigma}\right\}, \tag{4.5.92}$$

which is understood in the sense that F and Γ act on the flavor and spin indices of the third quark in each doublet $\mathcal{D}$, and the factor 3 counts the three possible permutations. The trace in the last equation goes over the doublet indices. It is useful to work out the flavor and spin matrix elements of the $SU(2)$ unit matrix and the Pauli matrix τ_3 for proton and neutron (use $\tau_3\,u = u$, $\tau_3\,d = -d$):

$$\mathbb{1}^{\uparrow\uparrow} = \mathbb{1}^{pp} = \mathbb{1}^{nn} = \begin{pmatrix}1&0\\0&1\end{pmatrix}, \qquad \tau_3^{\uparrow\uparrow} = \tau_3^{pp} = -\tau_3^{nn} = \begin{pmatrix}1&0\\0&-\frac{1}{3}\end{pmatrix}. \tag{4.5.93}$$

The matrix elements of the unit matrix are just those in (4.5.89). Their combination yields the two-flavor quark charge matrix, cf. Eq. (4.5.52):

$$\mathsf{Q} = \begin{pmatrix}q_u&0\\0&q_d\end{pmatrix} = \frac{\mathbb{1}}{6} + \frac{\tau_3}{2} \quad\Rightarrow\quad \mathsf{Q}^{pp} = \frac{2}{3}\begin{pmatrix}1&0\\0&0\end{pmatrix}, \quad \mathsf{Q}^{nn} = \frac{1}{3}\begin{pmatrix}-1&0\\0&1\end{pmatrix}, \tag{4.5.94}$$

from where one obtains the charges of proton and neutron:

$$\langle p\uparrow|\,\mathsf{Q}\,|p\uparrow\rangle = \frac{3}{2}\,\mathrm{Tr}\,\mathsf{Q}^{pp} = 1\,, \qquad \langle n\uparrow|\,\mathsf{Q}\,|n\uparrow\rangle = \frac{3}{2}\,\mathrm{Tr}\,\mathsf{Q}^{nn} = 0 \tag{4.5.95}$$

as well as their magnetic moments:

$$\begin{aligned} \langle p\uparrow|\,\mathsf{Q}\,\tau_3\,|p\uparrow\rangle &= \frac{3}{2}\,\mathrm{Tr}\left\{\mathsf{Q}^{pp}\,\tau_3^{\uparrow\uparrow}\right\} = 1\,, \\ \langle n\uparrow|\,\mathsf{Q}\,\tau_3\,|n\uparrow\rangle &= \frac{3}{2}\,\mathrm{Tr}\left\{\mathsf{Q}^{nn}\,\tau_3^{\uparrow\uparrow}\right\} = -\tfrac{2}{3}\,, \end{aligned} \tag{4.5.96}$$

apart from the remaining spatial integral. However, since the spatial part is taken to be identical for proton and neutron, the last relation yields the quark-model relation $\mu_n/\mu_p = -\frac{2}{3}$ which is quite close to the experimental value -0.685. Similarly, one can also work out the magnetic moments for the other ground-state octet members:

$$\mu_{\Sigma^+} = 1\,, \qquad \mu_{\Sigma^0} = \tfrac{1}{3}\,, \qquad \mu_{\Sigma^-} = \mu_{\Xi^-} = \mu_\Lambda = -\tfrac{1}{3}\,, \qquad \mu_{\Xi^0} = -\tfrac{2}{3}\,, \tag{4.5.97}$$

and in principle also those of the decuplet baryons.

References and further reading

Quark models:

- J. F. Donoghue, E. Golowich, B. R. Holstein, *Dynamics of the Standard Model*. Cambridge University Press, 1992
- A. W. Thomas, W. Weise, *The Structure of the Nucleon*. Wiley-VCH, 2001
- A. Hosaka, H. Toki, *Quarks, Baryons and Chiral Symmetry*. World Scientific, 2001.
- F. Jegerlehner, *Quantum Chromodynamics and strong interaction physics*. Lecture notes, 2009. http://www-com.physik.hu-berlin.de/~fjeger/books.html
- S. Capstick, W. Roberts, *Quark Models of Baryon Masses and Decays*, Prog. Part. Nucl. Phys. 45 (2000) 241, arXiv:nucl-th/0008028

Spontaneous chiral symmetry breaking:

- A. W. Thomas, W. Weise, *The Structure of the Nucleon*. Wiley-VCH, 2001
- S. Pokorski, *Gauge Field Theories*. Cambridge University Press, 1987
- V. P. Nair, *Quantum Field Theory: A Modern Perspective*. Springer, 2005
- C. D. Roberts, *Strong QCD and Dyson-Schwinger Equations*. Lecture notes, 2012. arXiv:1203.5341 [nucl-th]

Axial anomaly:

- S. Pokorski, *Gauge Field Theories*. Cambridge University Press, 1987
- J. F. Donoghue, E. Golowich, B. R. Holstein, *Dynamics of the Standard Model*. Cambridge University Press, 1992
- V. P. Nair, *Quantum Field Theory: A Modern Perspective*. Springer, 2005
- R. A. Bertlmann, *Anomalies in Quantum Field Theory*. Oxford University Press, 1996
- M. Kaku, *Quantum Field Theory: A Modern Introduction*. Oxford University Press, 1993

Chiral effective field theories:

- J. F. Donoghue, E. Golowich, B. R. Holstein, *Dynamics of the Standard Model*. Cambridge University Press, 1992
- A. W. Thomas, W. Weise, *The Structure of the Nucleon*. Wiley-VCH, 2001
- S. Pokorski, *Gauge Field Theories*. Cambridge University Press, 1987
- S. Scherer, *Introduction to Chiral Perturbation Theory*. Adv. Nucl. Phys. **27** (2003) 277. arXiv:hep-ph/0210398
- M. Birse and J. McGovern, *Chiral perturbation theory*. Appears in: F. Close, S. Donnachie and G. Shaw (ed.), *Electromagnetic interactions and hadronic structure*, Cambridge University Press, 2007
- J. D. Walecka, *Theoretical nuclear and subnuclear physics*. World Scientific, 1995

Hadron matrix elements:

- V. Barone, E. Predazzi, *High-Energy Particle Diffraction*. Springer, 2002
- V. Gribov, *Strong Interactions of Hadrons at High Energies*. Cambridge University Press, 2009
- F. Halzen, A. D. Martin, *Quarks and Leptons: An Introductory Course in Modern Particle Physics*. Wiley, 1984.
- A. W. Thomas, W. Weise, *The Structure of the Nucleon*. Wiley-VCH, 2001
- J. F. Donoghue, E. Golowich, B. R. Holstein, *Dynamics of the Standard Model*. Cambridge University Press, 1992